Ablation of solids by femtosecond lasers: ablation mechanism and ablation thresholds for metals and dielectrics — Source link ☒

Eugene G Gamaly, Andrei Rode, Barry Luther-Davies, Vladimir Tikhonchuk

Institutions: Australian National University

Topics: Laser ablation, Ablation, Femtosecond, Laser and Pulse duration

Related papers:

- Femtosecond, picosecond and nanosecond laser ablation of solids

- Nanosecond-to-femtosecond laser-induced breakdown in dielectrics

- Ablation of metals by ultrashort laser pulses

- Ultrashort-pulse laser machining of dielectric materials

- Laser-Induced Damage in Dielectrics with Nanosecond to Subpicosecond Pulses

Share this paper: 🟦 🐦 in ✉

View more about this paper here: https://typeset.io/papers/ablation-of-solids-by-femtosecond-lasers-ablation-mechanism-2a344832mu

Ablation of solids by femtosecond lasers: Ablation mechanism and ablation thresholds for metals and dielectrics

E. G. Gamaly, A. V. Rode, B. Luther-Davies, and V. T. Tikhonchuk

---

Articles you may be interested in

Nanochemical effects in femtosecond laser ablation of metals
Appl. Phys. Lett. **102**, 074107 (2013); 10.1063/1.4793521

Reflection of femtosecond laser light in multipulse ablation of metals
J. Appl. Phys. **110**, 043102 (2011); 10.1063/1.3620898

Ionization and fragmentation of solid C 60 by femtosecond laser ablation
J. Chem. Phys. **126**, 061101 (2007); 10.1063/1.2565642

Ultrasound generated by a femtosecond and a picosecond laser pulse near the ablation threshold
J. Appl. Phys. **98**, 033104 (2005); 10.1063/1.1999827

Microscopic mechanisms of ablation and micromachining of dielectrics by using femtosecond lasers
Appl. Phys. Lett. **82**, 4382 (2003); 10.1063/1.1583857

Ablation of solids by femtosecond lasers: Ablation mechanism and ablation thresholds for metals and dielectrics

E. G. Gamaly,[a] A. V. Rode, and B. Luther-Davies
Laser Physics Centre, Research School of Physical Sciences and Engineering, Australian National University, Canberra ACT 0200, Australia

V. T. Tikhonchuk
Institut de Physique Fondamentale, Universite Bordeaux 1, France

The mechanism of ablation of solids by intense femtosecond laser pulses is described in an explicit analytical form. It is shown that at high intensities when the ionization of the target material is complete before the end of the pulse, the ablation mechanism is the same for both metals and dielectrics. The physics of this new ablation regime involves ion acceleration in the electrostatic field caused by charge separation created by energetic electrons escaping from the target. The formulas for ablation thresholds and ablation rates for metals and dielectrics, combining the laser and target parameters, are derived and compared to experimental data. The calculated dependence of the ablation thresholds on the pulse duration is in agreement with the experimental data in a femtosecond range, and it is linked to the dependence for nanosecond pulses. © *2002 American Institute of Physics.* [DOI: 10.1063/1.1447555]

I. INTRODUCTION: THE ULTRA SHORT PULSE LASER-MATTER INTERACTION MODE

The rapid development of femtosecond lasers over the last decade has opened up a wide range of new applications in industry, material science, and medicine. One important physical effect is material removal or laser ablation by femtosecond pulses, which can be used for the deposition of thin films; the creation of new materials; for micro-machining; and even in the arts, for picture restoration and cleaning. Femtosecond laser ablation has the important advantage in such applications compared with ablation using nanosecond pulses because there is little or no collateral damage due to shock waves and heat conduction produced in the material being processed. In order to choose the optimal laser and target parameter it is useful to have simple scaling relations, which predict the ablation condition for an arbitrary material. In this paper we present an analytical description of the ablation mechanism and derive appropriate analytical formulas.

In order to remove an atom from a solid by the means of a laser pulse one should deliver energy in excess of the binding energy of that atom. Thus, to ablate the same amount of material with a shorter pulse one should apply higher laser intensity approximately in inverse proportion to the pulse duration. For example, laser ablation with 100 fs pulses requires an intensity in the range $\sim 10^{13} - 10^{14}$ W/cm^2,[1,2] while 30–100 ns pulse ablates the same material at the intensities $\sim 10^8 - 10^9$ W/cm^2.[3] At intensities above $10^{13} - 10^{14}$ W/cm^2 ionization of practically any target material takes place early in the laser pulse time. For example, if an intense, $10^{13} - 10^{14}$ W/cm^2, femtosecond pulse interacts with a dielectric, almost full single ionization of the target occurs at

the beginning of the laser pulse. Following ionization, the laser energy is absorbed by free electrons due to inverse Brehmstrahlung and resonance absorption mechanisms and does not depend on the initial state of the target. Consequently, the interaction with both metals and dielectrics proceeds in a similar way, which contrasts to the situation with a long pulse where ablation of metals occurs at relatively low intensity compared with that for a transparent dielectric whose absorption is negligibly small.

Another distinctive feature of the ultra short interaction mode is that the energy transfer time from the electrons to ions by Coulomb collisions is significantly longer (picoseconds) than the laser pulse duration ($t_p \sim 100$ fs). Therefore, the conventional hydrodynamics motion does not occur during the femtosecond interaction time.

There are two forces which are responsible for momentum transfer from the laser field and the energetic electrons to the ions in the absorption zone: one is due to the electric field of charge separation and another is the ponderomotive force. The charge separation occurs if the energy absorbed by the electrons exceeds the Fermi energy, which is approximately a sum of the binding energy and work function, so the electrons can escape from the target. The electric field of charge separation pulls the ions out of the target. At the same time, the ponderomotive force of the laser field in the skin layer pushes electrons deeper into the target. Correspondingly it creates a mechanism for ion acceleration into the target. Below we demonstrate that the former mechanism dominates the ablation process for sub-picosecond laser pulses at an intensity of $10^{13} - 10^{14}$ W/cm^2. This mechanism of material ablation by femtosecond laser pulses is quite different from the thermal ablation by long pulses.

Femtosecond ablation is also sensitive to the temporal and spatial dependence of the intensity of the laser pulse.

---

[a]Telephone: ++61-2-6125-0171; fax: ++61-2-6125-0732; electronic mail: gam110@rsphysse.anu.edu.au

The chirped pulse amplification (CPA) technique commonly used for short pulse generation[4] can produce a main (short) pulse accompanied by a nanosecond pre-pulse or pedestal that can be intense enough itself to ablate the target. Therefore, an important condition for the practical realization of the pure femtosecond interaction mode should be that the intensity in any pre-pulse has to be lower than the thresholds for ablation or ionization in the nanosecond regime. There are fortunately several methods for achieving high pulse contrast (nonlinear absorbers, conversion to second harmonic, etc.).[5,8]

A rather simple and straightforward analytical model can describe the ultra short pulse mode of laser-matter interaction. The main features of this model were developed more than 10 years ago in connection with the ultra short and super intense laser-matter interaction.[6–8] In what follows this model is modified and applied to the problems of the laser ablation at relatively moderate intensities near the ablation threshold for solids. The absorption coefficient, ionization and ablation rates, and ablation thresholds for both metals and dielectrics are expressed in terms of the laser and target parameters by explicit formulas. The comparison to the long-pulse interaction mode and to the experimental data is presented and discussed.

II. LASER FIELD PENETRATION INTO A TARGET: TRANSIENT SKIN-EFFECT

The pulse duration in the sub-picosecond laser interaction with a solid target appears to be shorter than all characteristic relaxation times: the electron-to-ion energy transfer time, the electron heat conduction time, and therefore the hydrodynamic or, the expansion time. Thus, the femtosecond laser pulse interacts with a solid target with a density remaining almost constant during the laser pulse. The major process during the laser-target interaction is the electron heating by the laser field. The laser electromagnetic field in the target can be found as a solution to Maxwell equations coupled to the material equations. The solution is straightforward when the material parameters are constant in time and space and independent on the incident intensity. In this case the interaction falls in framework of well-known skin-effect.[7–9] However, in the femtosecond laser-matter interaction the electron number density n_e (and thus the plasma frequency ω_{pe}), the effective electron collision frequency ν_{eff}, the absorption coefficient A, and the skin-depth l_s, all are the functions of the laser intensity and time. A self-consistent solution for the coupled field and material equations becomes rather complicated. In order to obtain physically sound scaling relations we use an alternative way. We employ the exponential dependence of the laser electric field $E(x)$ with depth in a solid target $E(x) = E(0)\exp[-x/l_s]$, as for the normal skin-effect; here l_s is the field penetration length (skin-depth). We suppose that the target fills half-space at $x > 0$. The skin-depth, $l_s = (c/\omega k)$ is conventionally expressed through the imaginary part of the refractive index **k** and the laser frequency ω.[9,10] The dielectric function in the Drude approximation describes well the initial solid state as well as the ionized state just before ablation:

$$\varepsilon = 1 - \frac{\omega_{pe}^2}{\omega(\omega + i\nu_{eff})} = \varepsilon' + i\varepsilon'', \quad \varepsilon^{1/2} = n + ik; \quad (1)$$

here $\omega_{pe} = (4\pi e^2 n_e/m_e)^{1/2}$ is the electron plasma frequency, and ν_{eff} is an effective collision frequency of electrons with a lattice (ions) that is defined below.

The main difference between the ultra short laser-matter interaction mode and the conventional low-intensity case resides in the fact that the plasma frequency, the effective collision frequency, and thus, the real and imaginary parts of the dielectric permittivity, all are intensity and time-dependent. In what following we find the dependencies of all material parameters on the electron and lattice temperature for the conditions close to the ablation threshold. Then we obtain the electron temperature dependence on the laser intensity and time by using the conventional skin-effect solution for the electric field in a target. We also determine the conditions when the approximations used are valid. The finding of these dependencies is the subject of the next sections.

III. INTENSITY THRESHOLD FOR IONIZATION OF DIELECTRICS

The large real and small imaginary parts characterize the dielectric function in dielectrics at the low intensity of the electric field. The imaginary part increases mainly due to ionization. There are two major mechanisms of ionization in the laser field: ionization by electron impact (avalanche ionization); and the multiphoton ionization. The time dependence of the number density of free electrons n_e stripped off the atoms by these processes is defined by the rate equation:[1,11]

$$\frac{dn_e}{dt} = n_e w_{imp} + n_a w_{mpi}; \quad (2)$$

here n_a is the density of neutral atoms, w_{imp} is the time independent probability (in s^{-1}) for the ionization by electron impact, and w_{mpi} is the probability for the multiphoton ionization.[8,11,12] For the case of single ionization it is convenient to present the probabilities w_{imp} and w_{mpi}, in the form:

$$w_{imp} \approx \frac{\varepsilon_{osc}}{J_i}\left(\frac{2\omega^2\nu_{eff}}{\omega^2 + \nu_{eff}^2}\right), \quad (3)$$

$$w_{mpi} \approx \omega n_{ph}^{3/2}\left(\frac{\varepsilon_{osc}}{2J_i}\right)^{n_{ph}}; \quad (4)$$

here ε_{osc} is the electron quiver energy in the laser field, $n_{ph} = J_i/\hbar\omega$ is the number of photons necessary for atom ionization by the multiphoton process, J_i is the ionization potential, and ν_{eff} is the effective collision frequency. It must be emphasized that the effective collision frequency in Eq. (3) accounts for the inelastic collisions leading to the energy gain by the electrons. In general, it differs from the effective collision frequency in Eq. (1) and in the sections below, which accounts for the momentum exchange due to elastic collisions.

One can see from Eqs. (3) and (4) that the relative role of the impact and multiphoton ionization depends dramatically on the relation between the electron quiver energy

and the ionization potential. If $\varepsilon_{osc} > J_i$ then $w_{mpi} > w_{imp}$, and the multiphoton ionization dominates for any relationship between the frequency of the incident light and the efficient collision frequency. By presenting the oscillation energy in a scaling form:

$$\varepsilon_{osc}[\text{eV}] = 9.3(1+\alpha^2)\frac{I}{10^{14}[\text{W/cm}^2]}(\lambda[\mu\text{m}])^2; \qquad (5)$$

here α accounts for the laser polarization ($\alpha = 1$ for the circular and $\alpha = 0$ for the linear polarization), it is evident that the multiphoton ionization dominates in the laser-interaction at intensities above 10^{14} W/cm^2 (for the 100 fs pulse duration this condition corresponds to the laser fluence of 10 J/cm^2).

The general solution to Eq. (2) with the initial condition $n_e(t=0) = n_0$ is the following:

$$n_e(I,\lambda,t) = \left\{ n_0 + \frac{n_a w_{mpi}}{w_{imp}}[1 - \exp(-w_{imp}t)] \right\}$$
$$\times \exp(w_{imp}t). \qquad (6)$$

It is in a good agreement with the direct numerical solution to the full set of kinetic equations.[1] Electron impact ionization is the main ionization mechanism in the long (nanosecond) pulse regime. Then $\varepsilon_{osc} \ll J_i$ and $\omega \ll \nu_{eff}$, and one can neglect the second term in Eq. (6) and the number of free electrons exponentially increases with the product of w_{imp} and the pulse duration: $n_e \sim n_0 \exp\{w_{imp} \times t_p\}$. Therefore in the long-pulse regime the ionization threshold depends on the laser fluence $F = I \times t_p$. In the case of high intensities multiphoton ionization dominates and the number of free electrons increases linearly with time: $n_e \sim n_a w_{mpi}t$. The ionization time could be shorter than the pulse duration and the ionization threshold depends on the laser intensity and laser wavelength. It is conventional to suggest that the ionization threshold (or breakdown threshold) be achieved when the electron number density reaches the critical density corresponding to the incident laser wavelength.[11,13] The ionization threshold for the majority of materials lies at intensities in between $(10^{13}-10^{14})$ W/cm^2 ($\lambda \sim 1~\mu$m) with a strong non-linear dependence on intensity. For example, for a silica target at the intensity 2×10^{13} W/cm^2 avalanche ionization dominates, and the first ionization energy is not reached by the end of the 100 fs pulse at 1064 nm. At 10^{14} W/cm^2 multiphoton ionization dominates and the full first ionization is completed after 20 fs. When the ionization is complete, the plasma formed in the skin-layer of the target has a free-electron density comparable to the ion density of about 10^{23} cm^{-3}. Hence, for the derivation of scaling relations the electron number density (and thus the electron plasma frequency) can be considered as being constant. It should be also mentioned that the ionization threshold decreases with the increase in the photon energy.

IV. ELECTRON COLLISION FREQUENCY AND ENERGY TRANSFER FROM ELECTRONS TO IONS

In order to meet the ablation conditions the average electron energy should increase from the initial room tempera-

ture up to the Fermi energy ε_F, i.e., up to several eV. The electron–electron equilibration time is of the order of magnitude of the reciprocal electron plasma frequency, i.e., $\sim \omega_{pe}^{-1} \sim 10^{-2}$ fs that is much shorter than the pulse duration. Therefore the electron energy distribution during the heating process is close to equilibrium and follows the laser intensity evolution in time adiabatically adjusting to any changes.

The electron-ion collision frequency changes from the low-temperature limit, when the electron-phonon interaction is dominated by the lattice temperature,[12] to the high-energy limit, where the electron-ion interaction is dominated by the electron temperature.[13] The electron gas is nonideal in the high-density conditions: the energy of Coulomb interaction is comparable to the electron kinetic energy and there are only few electrons in the Debye sphere. There are no reliable analytical expressions for the effective electron collision frequency in the whole energy-density domain from low to high temperatures. There are interpolation formulas for some materials are given in Ref. 14, and interpolation for Al is given in Ref. 15. Physically sound estimates could also be made for the maximum collision frequency near the Fermi energy and therefore, close to the conditions for the ablation threshold.

In the low-temperature limit $T_D \ll T \ll T_F$ electron-phonon collisions dominate (T_D is the Debye temperature). The probability for an electron to emit or to absorb a phonon can be estimated at $T > T_D$ as follows:[9,12]

$$\nu_{e-ph} \approx \left(\frac{m_e}{M}\right)^{1/2}\frac{J_i}{\hbar}\frac{T}{T_D}. \qquad (7)$$

Taking for example $J_i = 7.7$ eV (first ionization potential for copper), $T_D(\text{Cu}) \sim 300$ K, and $M_{\text{Cu}} = 63.54$ a.m.u. one obtains $\nu_{eff} \sim 9 \times 10^{15}$ s^{-1}. This estimate is very close to the effective frequency at room temperature of 8.6×10^{15} s^{-1} extracted from conductivity measurements (see Ref. 16).

In the opposite high-temperature limit the effective frequency of electron-ion Coulomb collisions decreases with the electron temperature. Thus, the effective collision frequency has maximum at the temperature approaching the Fermi energy.

At high temperatures $T_e \gg \varepsilon_F$ the effective electron-ion collision frequency could be estimated by using the model for ideal plasma at solid state density. The collision is considered as a 90-deg deflection of an electron path due to the Coulomb interaction with the ion, and the collision frequency is the frequency of the momentum exchange. According to Ref. 13:

$$\nu_{ei} \approx 3 \times 10^{-6}\ln\Lambda\frac{n_e Z}{T_{eV}^{3/2}}. \qquad (8)$$

For example, from Eq. (8) the electron-ion collision frequency in copper at the electron temperature coinciding with the Fermi energy ($n_e = 0.845 \times 10^{23}$ cm^{-3}, $\omega_p = 1.64 \times 10^{16}$ s^{-1}, $T_{eV} \sim 7.7$ eV, $\ln\Lambda \sim 2$) is $\nu_{ei} = 2.38 \times 10^{16}$ s^{-1}. This value is about twice higher than that estimated from the low-temperature case, and almost coincides with the plasma frequency, $\nu_{eff} \sim \omega_{pe} = 2.39 \times 10^{16}$ s^{-1}. The discussion and interpolation in Ref. 15 gives the maximum of the efficient

collision frequency for aluminum also close to ω_{pe}. Therefore, it seems reasonable to assume that $\nu_{\text{eff}} \approx \omega_{pe}$ for the further estimates of the ablation threshold, as it has been also suggested in Ref. 1. The value of ν_{eff} can be corrected by experimental measurements of the skin depth (ablation depth).

Thus, in the ablation conditions the inequality holds $\nu_{ei} \gg \omega$. Therefore the electron mean free path is much smaller than the skin depth. That is, the condition for the normal skin effect is valid, and one can use the exponential spatial dependence for the field. The electron-ion energy transfer time in dense plasma can be expressed through the collision frequency Eq. (7) or (8) as follows:

$$\tau_{ei} \approx \frac{M}{m_e} \nu_{ei}^{-1}. \qquad (9)$$

The estimation for copper yields the ion heating time $\tau_{ei} = 4.6 \times 10^{-12}$ s, which is in agreement with the values suggested by many authors.[1,8,15,17] A similar estimate for silica gives 6.4×10^{-12} s. Therefore, for the sub-picosecond pulses ($t_p \sim 100$ fs) the ions remain cold during the laser pulse interaction with both metals and dielectrics, and one can use a steplike density profile for laser absorption calculations.

V. ABSORPTION MECHANISM, ABSORPTION COEFFICIENT, AND ABSORPTION DEPTH

At intensities above 10^{14} W/cm^2 the ionization time for a dielectric is just a few femtoseconds, typically much shorter than the pulse duration (~ 100 fs). The electrons produced by ionization in dielectrics then dominate the absorption in the same way as the free carriers in metals, and the characteristics of the laser-matter interaction become independent of the initial state of the target. As a result, the inverse Bremsstrahlung and resonant absorption (for p-polarized light at oblique incidence) become the dominant absorption mechanisms for both metals and dielectrics.

We have shown in the previous sections that near the ablation threshold the conditions hold: $\nu_{\text{eff}} \sim \omega_{pe} > \omega$. The dielectric function and refractive index then are as the follows:

$$\varepsilon' \approx \frac{\omega^2}{\omega_{pe}^2}, \quad \varepsilon'' \approx \frac{\omega_{pe}}{\omega}\left(1 + \frac{\omega^2}{\omega_{pe}^2}\right)^{-1}, \quad n \approx k = \left(\frac{\varepsilon''}{2}\right)^{1/2}. \qquad (10)$$

The absorption coefficient then immediately follows from the Fresnel formulas:[10]

$$A = 1 - R \approx \frac{4n}{(n+1)^2 + n^2}. \qquad (11)$$

The ratio of the absorption coefficient to the skin length that enters into calculations of the electron temperature below is a weak function of material properties.[7,8] This ratio reads

$$\frac{A}{l_s} \approx \frac{2\omega}{c}\left(1 + \frac{1}{n} + \frac{1}{2n^2}\right)^{-1}. \qquad (12)$$

The function in brackets depends weakly on the material and laser parameters. For example, for copper ablation at 780 nm ($\omega = 2.415 \times 10^{15}$ s^{-1}; $\omega_{pe} = 1.64 \times 10^{16}$ s^{-1}) it comprises 0.585, while for gold target ablation at 1064 nm ($\omega = 1.79$

$\times 10^{15}$ s^{-1}; $\omega_{pe} = 1.876 \times 10^{16}$ s^{-1}) it amounts to 0.65. Thus, we assume in further calculations that $A/l_s = 2\omega/c = 4\pi/\lambda$.

VI. ELECTRON HEATING IN THE SKIN LAYER

In the previous section we have demonstrated that electrons have no time to transfer the energy to the ions during the laser pulse $\tau_{ei} > t_p$. That means that the target density remains unchanged during the laser pulse. The electrons also cannot transport the energy out of the skin layer because the heat conductivity time is much longer than the pulse duration. It is easy to see that the electron heat conduction time t_{heat} (the time for the electron temperature smoothing across the skin-layer l_s) is also much longer than the pulse duration. Indeed, the estimates for this time with the help of conventional thermal diffusion[9] give

$$t_{\text{heat}} \approx \frac{l_s^2}{\kappa}, \quad \kappa = \frac{l_e \nu_e}{3},$$

where κ is the coefficient of thermal diffusion, l_e and ν_e are the electron mean free path and velocity, respectively. Using copper as an example yields $l_s = 67.4$ nm, $\kappa \sim 1$ cm^2/s, and the electron heat conduction time is in the order of tens of picoseconds.

The energy conservation law takes then a simple form of the equation for the change in the electron energy (or temperature T_e) due to absorption in a skin layer:[6–8]

$$c_e(T_e)n_e\frac{\partial T_e}{\partial t} = -\frac{\partial Q}{\partial x}, \quad Q = AI_0 \exp\left\{-\frac{2x}{l_s}\right\}; \qquad (13)$$

here Q is the absorbed energy flux in the skin layer, $A = I/I_0$ is the absorption coefficient, $I_0 = cE^2/4\pi$ is the incident laser intensity, n_e and c_e are the number density and the specific heat of the conductivity electrons. In general, Eq. (13) describes the electron heating by the laser field in a solid with the time-dependent parameters, $c_e(t)$, $A(t)$, $l_s(t)$, $n_e(t)$. However, we can simplify Eq. (13) by using the following physical arguments. First, the electron specific heat increases with electron temperature from the low-temperature degenerate state $c_e = \pi^2 T_e/2\varepsilon_F$ for $T_e \ll \varepsilon_F$,[16] up to the maximum value of $c_e \sim 3/2$ for the conventional ideal gas at high temperature $T_e \sim \varepsilon_F$. We take the same specific heat as for the ideal gas in Eq. (13) because the target becomes fully ionized early in the laser pulse and the electrons are in conditions close to that of the ideal gas. For the same reason, the electron number density rapidly increases in the beginning of the pulse and for the rest of the pulse it remains almost constant. It was shown in the previous section that the ratio of the absorption coefficient to the skin depth is also time-independent. Thus, the only approximation we make in order to obtain a convenient scaling relations is neglecting the time dependence of the skin depth in the exponent while time-integrating Eq. (13). This integration yields time and space dependencies of the electron temperature in the skin layer:

$$T_e = \frac{4}{3}\frac{AI_0 t}{l_s n_e} \exp\left\{-\frac{2x}{l_s}\right\}, \quad T_e \approx \varepsilon_F. \qquad (14)$$

Phys. Plasmas, Vol. 9, No. 3, March 2002

Ablation of solids by femtosecond lasers . . .   953

The relationship Eq. (14) represents an appropriate scaling law for the electron temperature in the skin layer. The experimental data correlate well with the prediction of Eq. (14). For example, the estimate of the skin depth in a copper target irradiated by a Ti:sapphire laser ($\lambda = 780$ nm, $\omega = 2.4 \times 10^{15}$ s^{-1}; $\nu_{\text{eff}} \approx \omega_{pe} = 1.639 \times 10^{16}$ s^{-1}, $n_e = 0.845 \times 10^{23}$ cm^{-3}) gives $l_s = 69$ nm. The maximum electron temperature at the surface of the copper target under the fluence $AI_0 t_p = 1$ J/cm^2 reaches $T_e = 7.5$ eV, which is close to the Fermi energy for copper.

VII. ABLATION MECHANISM: IONS PULLED OUT OF THE TARGET BY ENERGETIC ELECTRONS

It was shown in the preceding section that the free electrons in the skin layer can gain the energy exceeding the threshold energy required to leave a solid target during the pulse time. The energetic electrons escape the solid and create a strong electric field due to charge separation with the parent ions. The magnitude of this field depends directly on the electron kinetic energy $\varepsilon_e \sim (T_e - \varepsilon_{esc})$ (ε_{esc} is the work function) and on the gradient of the electron density along the normal to the target surface (assuming one dimensional expansion):[9,18]

$$E_a = -\frac{\varepsilon_e(t)}{e}\frac{\partial \ln n_e}{\partial z}. \tag{15}$$

A ponderomotive force of the electric field in the target is another force applied to the ions during the laser pulse:[19]

$$F_{pf} = -\frac{2\pi e^2}{m_e c \omega^2}\nabla I \cong \frac{I}{2n_e c l_s}\frac{\omega_{pe}^2}{\omega^2}. \tag{16}$$

Let us compare the force in the electrostatic field of the space charge to the ponderomotive force of the laser wave. The electrostatic force $F_{el\text{-}st}$ can be evaluated using Eq. (15) and taking into account that the characteristic space scale is Debye length $l_D \sim v_e/\omega_{pe}$, where $v_e = [(T_e - \varepsilon_{esc})/m_e]^{1/2}$ is the electron thermal velocity:

$$F_{el\text{-}st} = eE_a = -\varepsilon_e(t)\frac{\partial \ln n_e}{\partial z} \cong \frac{It}{n l_s l_D}. \tag{17}$$

This force depends on time explicitly through the electron energy. It increases during the laser pulse. The ratio of two forces at the end of the laser pulse reads

$$\left|\frac{F_{pf}}{F_{el\text{-}st}}\right| \cong \frac{1}{2\omega t_p}\left(\frac{\omega_{pe}}{\omega}\right)\left(\frac{v_e}{c}\right). \tag{18}$$

For a solid state density plasma $\omega_{pe}/\omega \sim 10$; $\omega > 10^{15}$ s^{-1}; and for $t_p \sim 100$ fs the ratio Eq. (18) is much less than 1, so the ponderomotive force can be neglected for the calculation of the ablation threshold. However, both electrostatic and ponderomotive forces are of the same order of magnitude at the beginning of the laser pulse, and both forces should be taken into account in calculations of the electron energy.

The field Eq. (15) pulls the ions out of the solid target if the electron energy is larger than the binding energy ε_b of ions in the lattice. The maximum energy of ions dragged from the target reaches $\varepsilon_i(t) \approx Z\varepsilon_e(t) \approx (T_e - \varepsilon_{esc} - \varepsilon_b)$. The

time necessary to accelerate and ablate ions could be estimated with the help of the equation for the change of ion momentum:

$$\frac{dp_i}{dt} \approx eE_a. \tag{19}$$

The ion acceleration time, i.e., the time required for the ion to acquire the energy of ε_e could be found with the help of Eq. (19) as follows:

$$t_{acc} = \frac{l_D}{v_i} \approx \frac{2}{\omega_{pe}}\left(\frac{m_i}{m_e}\right)^{1/2}\left(\frac{T_e - \varepsilon_{esc}}{T_e - \varepsilon_{esc} - \varepsilon_b}\right)^{1/2}. \tag{20}$$

Below the ablation threshold, when $T_e \sim \varepsilon_{esc} + \varepsilon_b$ the acceleration time is much longer than the pulse duration. However, when the laser fluence exceeds the ablation threshold this time is comparable and even shorter than the pulse duration. For example, for copper at $F = 1$ J/cm^2 this time is less than 40 fs. This means that for high intensities (fluences) well over the ablation threshold Eq. (13) for the electron temperature should include the energy losses for ion heating. This effect of electrostatic acceleration of ions is well known from the studies of the plasma expansion[9,18] and ultrashort intense laser-matter interaction.[8]

A. Ablation threshold for metals

According to Eq. (20), the minimum energy that the electron needs to escape the solid equals the work function. In order to drag the ion out of the target the electron must have an additional energy equal to or larger than the ion binding energy. Hence, the ablation threshold for metals can be defined as the following condition: the electron energy must reach, in a surface layer $d \ll l_s$ by the end of the laser pulse, the value equal to the sum of the atomic binding energy and the work function. Using Eq. (14) for the electron temperature we obtain the energy condition for the ablation threshold:

$$\varepsilon_e = \varepsilon_b + \varepsilon_{esc} = \frac{4}{3}\frac{AI_0 t_p}{l_s n_e}. \tag{21}$$

The threshold laser fluence for ablation of metals is then defined as the following:

$$F_{th}^m \equiv I_0 t_p = \frac{3}{4}(\varepsilon_b + \varepsilon_{esc})\frac{I_s n_e}{A}. \tag{22}$$

We assume that the number density of the conductivity electrons is unchanged during the laser-matter interaction process. After insertion $A/l_s = 4\pi/\lambda$ into Eq. (22) the approximate formula for the ablation threshold takes the following form:

$$F_{th}^m \equiv I_0 t_p \approx \frac{3}{8}(\varepsilon_b + \varepsilon_{esc})\frac{c n_e}{\omega} \equiv \frac{3}{8}(\varepsilon_b + \varepsilon_{esc})\frac{\lambda n_e}{2\pi}. \tag{23}$$

The formula Eq. (23) predicts that the threshold fluence is proportional to the laser wavelength: $F_{th} \sim \lambda$. We demonstrate below that this relation agrees well with the experimental data.

B. Ablation threshold for dielectrics

The ablation mechanism for the ionized dielectrics is similar to that for metals. However, there are several distinctive differences. First, an additional energy is needed to create the free carriers, i.e., to transfer the electron from the valence band to the conductivity band. Therefore, the energy equal to the ionization potential J_i, should be delivered to the valence electrons. Second, the number density of free electrons depends on the laser intensity and time during the interaction process as has been shown in Sec. IV. However, if the intensity during the pulse exceeds the ionization threshold then the first ionization is completed before the end of the pulse, and the number density of free electrons saturates at the level $n_e \sim n_a$, where n_a is the number density of atoms in the target. Then the threshold fluence for ablation of dielectrics, taking into account the above corrections, is defined as the following:

$$F_{th}^d = \frac{3}{4}(\varepsilon_b + J_i)\frac{l_s n_e}{A}. \tag{24}$$

Therefore, as a general rule, the ablation threshold for dielectric in the ultra short laser-matter interaction regime must be higher than that for the metals, assuming that all the atoms in the interaction zone are at least singly ionized. Because the absorption in the ionized dielectric also occurs in a skin layer, one can use the relation $l_s/A \approx \lambda/4\pi$ for rough estimates and scaling relations.

Another feature of the defined above ablation thresholds Eqs. (23) and (24) is that they do not depend explicitly on the pulse duration and intensity. However, it is just a first order approximation. A certain, though weak, dependence is hidden in the absorption coefficient and in the number density of free electrons.

VIII. COMPARISON TO THE LONG PULSE REGIME

It is instructive to compare the above defined ablation threshold to that for the long laser pulses. This also helps in considering a general picture of the ablation process in a whole range of laser pulse duration.

The ultra short pulse laser-matter interaction mode corresponds to conditions when the electron-to-ion energy transfer time and the heat conduction time exceed significantly the pulse duration, $\tau_{ei} \sim t_{heat} \gg t_p$. Then the absorbed energy is going into the electron thermal energy, and the ions remain cold $\varepsilon_{ion} \ll \varepsilon_e$, making the conventional thermal expansion inhibited. However, as shown above, if the laser intensity is high enough, the electrons can gain the energy in excess of the Fermi energy and escape from the target. The electromagnetic field of the charge separation created by the escaped electrons pulls the ions out of the target. Hence, the extreme nonequilibrium regime of material ablation takes place. This regime occurs at the laser pulse duration $t_p < 200$ fs and at the intensities above $10^{13} - 10^{14}$ W/cm^2. The escaped electrons accelerate the ions by the electrostatic field of charge separation.

An intermediate regime takes place at the laser pulse duration 0.5 ps $< t_p < 100$ ps and at the intensities less than 10^{11} W/cm^2, when $\tau_{ei} \sim t_{heat} \sim t_p$ and $T_e \sim T_i$. The most appropriate description of the heating and expansion processes in this regime is given by the conventional two-temperature approach.[20]

At the longer laser pulse duration $t_p > 10$ ps the heat conduction and hydrodynamic motion dominate the ablation process, $t_p \gg \{\tau_{ei}; t_{heat}\}$. The electrons and the lattice (the ions) are in equilibrium early in the beginning of the laser pulse $T_e \sim T_i$. Hence, the limiting case of thermal expansion (thermal ablation) is suitable for the description of the long pulse ablation mode. The ablation threshold for this case is defined by condition that the absorbed laser energy $A I_0 t_p$, is fully converted into the energy of broken bonds in a layer with the thickness of the heat diffusion depth $l_{heat} \sim (\kappa t_p)^{1/2}$ during the laser pulse:[20]

$$A I_0 t_p \cong (\kappa t_p)^{1/2} \varepsilon_b n_a. \tag{25}$$

The well-known $t_p^{1/2}$ time dependence for the ablation fluence immediately follows from this equation:

$$F_{th} \approx \frac{(\kappa t_p)^{1/2} \varepsilon_b n_a}{A}. \tag{26}$$

Equations (23), (24), and (26) represent two limits of the short and the long pulse laser ablation with a clear demonstration of the underlying physics. The difference in the ablation mechanisms for the thermal long pulse regime and the nonequilibrium short pulse mode is two-fold.

First, the laser energy absorption mechanisms are different. The intensity for the long pulse interaction is in the range $10^8 - 10^9$ W/cm^2 with the pulse duration change from nanoseconds to picoseconds. The ionization is negligible, and the dielectrics are almost transparent up to the UV range. The absorption is weak, and it occurs due to the interband transitions, defects and excitations. At the opposite limit of the femtosecond laser-matter interaction the intensity is in excess of 10^{13} W/cm^2 and any dielectric is almost fully ionized in the interaction zone. Therefore, the absorption due to the inverse Bremsstrahlung and the resonance absorption mechanisms on free carriers dominates the interaction, and the absorption coefficient amounts to several tens percent.

Second, the electron-to-lattice energy exchange time in a long pulse ablation mode is of several orders of magnitude shorter than the pulse duration. By this reason the electrons and ions are in equilibrium, and ablation has a conventional character of thermal expansion. By contrast, for the short pulse interaction the electron-to-ion energy exchange time, as well as the heat conduction time, is much larger than the pulse duration, and the ions remain cold. Electrons can gain energy from the laser field in excess of the Fermi energy, and escape the target. The electric field of a charge separation pulls ions out of the target thus creating an efficient nonequilibrium mechanism of ablation.

IX. ABLATION DEPTH AND EVAPORATION RATE

The depth of a crater $x = d_{ev}$, drilled by the ultra short laser with the fluence near the ablation threshold $F = I_0 t > F_{th}$ is of the order of the skin depth. According to Eq. (14), it increases logarithmically with the fluence:

$$d_{ev} = \frac{l_s}{2} \ln \frac{F}{F_{th}}, \tag{27}$$

due to the exponential decrease of the incident electric field and electron temperature in the target material. Equation (27) coincides apparently with that from Ref. 21. However, one should note the difference in definitions of the threshold fluence and skin depth in this paper from that in Ref. 21. The skin depth calculated above for the laser interaction with copper target of 69 nm qualitatively complies with the ablation depth fitting to the experimental value of 80 nm given in Ref. 21.

The average evaporation rate, which is the number of particles evaporated per unit area per second, can be estimated using the energy conservation law for the ultra short interaction mode in the same way as it was done for the long pulses. Namely, the total absorbed laser energy flux in the optimum ablation mode balances by the outflow of ablated atoms times the energy expenses per atom that approximately equals to the Fermi energy. Thus, the ablation rate for the ultra short regime reads

$$(n\nu)_{short} \approx \frac{AI}{\varepsilon_F}. \tag{28}$$

Taking as a characteristic parameters for the ultra short mode $AI \sim 10^{14}$ W/cm^2 and $\varepsilon_F \sim 10$ eV, one obtains from Eq. (28) the typical ablation rate $\sim 6 \times 10^{30}$ l/cm^{2}s. Similarly, the evaporation rate for the long pulse regime is as follows:[3,20]

$$(n\nu)_{long} \approx \frac{I_a}{\varepsilon_b}. \tag{29}$$

Taking $I_a \sim 10^9$ W/cm^2 and $\varepsilon_b \sim 4$ eV,[3] the characteristic ablation rate for the long pulse regime of $\sim 3 \times 10^{27}$ l/cm^{2}s is about 2×10^3 times lower.

The number of particles evaporated per short pulse $(n\nu)S_{foc}t_p$ (S_{foc} is the focal spot area) is of several orders of magnitude lower than that for a long pulse. This effect eliminates the major problem in the pulsed laser deposition of the thin films, which is formation of droplets and particulates on the deposited film. The effect has been experimentally observed with 60 ps pulses and 76 MHz repetition rate by producing diamondlike carbon films with the rms surface roughness on the atomic level.[3]

One also can introduce the number of particles evaporated per Joule of absorbed laser energy as a characteristic of ablation efficiency. One can easily estimate that this characteristic is comparable for both the short-pulse and the long-pulse regimes.

X. COMPARISON TO THE EXPERIMENTAL DATA

Let us now to compare the above formulas to the different experimental data. Where it is available we present the full span of pulse durations from femtosecond to nanosecond range for ablation of metals and dielectrics.

A. Metals

Let us apply Eq. (23) for calculation of the ablation threshold for copper and gold targets ablated by a 780 nm
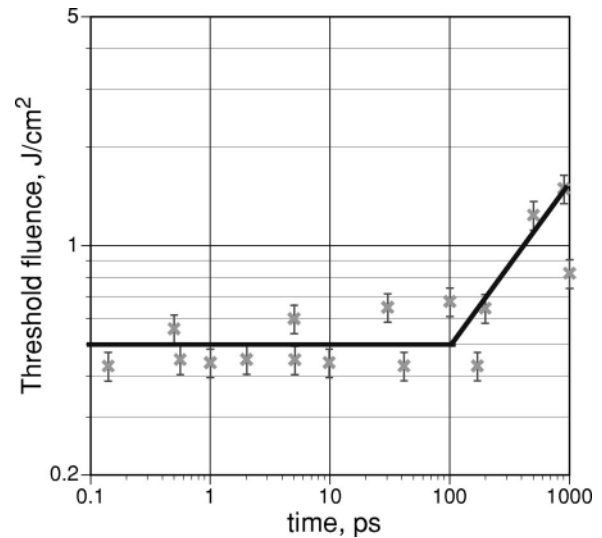

FIG. 1. Threshold laser fluence for ablation of gold targets (mirror and grating) versus laser pulse duration. The experimental points are from Ref. 22.

laser. The copper parameters are: density 8.96 g/cm^3, binding energy, e.g., heat of evaporation per atom $\varepsilon_b = 3.125$ eV/atom, $\varepsilon_{esc} = 4.65$ eV/atom, $n_a = 0.845 \times 10^{23}$ cm^{-3}. The calculated threshold $F_{th} \sim 0.51$ J/cm^2 (for $A \cong 1$) is in agreement with the experimental figure 0.5–0.6 J/cm^2 given in Ref. 21, though the absorption coefficient was not specified. For the long pulse ablation taking into account thermal diffusivity of copper 1.14 cm^2/s Eq. (26) predicts $F_{th}[\text{J/cm}^2] = 0.045 \times (t_p[\text{ps}])^{1/2}$.

For a gold target ($\varepsilon_b = 3.37$ eV/atom, $\varepsilon_{esc} = 5.1$ eV, $n_a = 5.9 \times 10^{22}$ cm^{-3}) evaporated by laser wavelength 1053 nm the ablation threshold from Eq. (23) is $F_{th} = 0.5$ J/cm^2. That figure should be compared to the experimental value of 0.45 ± 0.1 J/cm^2.[22] For the long pulse ablation assuming the constant absorption coefficient of $A = 0.74$ one finds from Eq. (26) $F_{th}[\text{J/cm}^2] = 0.049 \times (t_p[\text{ps}])^{1/2}$. We should note here that for the long pulse we take 1.3 cm^2/s for thermo-diffusivity value, which corresponds to equilibrium conditions with ion-dominated heat capacity. The experimental points from Ref. 22 and the calculated curve are presented in Fig. 1.

B. Silica

An estimate for the ablation threshold for silica from Eq. (24) taking $n_e \cong 7 \times 10^{22}$ cm^{-3}, $(\varepsilon_b + J_i) \cong (3.7 + 13.6)$ eV[25] by a laser with $\lambda = 1.053$ μm [$\omega = 1.79 \times 10^{15}$ s^{-1}; and $l_s/A \sim 1.6 \times 10^{-5}$ cm—see Eq. (12)] gives $F_{th} = 2.35$ J/cm^2, which is in a qualitative agreement with the experimental figures $\sim 2 \pm 0.5$ J/cm^2.[1] Formula Eq. (24) also predicts the correct wavelength dependence of the threshold: $F_{th} = 1.84$ J/cm^2 for $\lambda = 825$ nm and $F_{th} = 1.17$ J/cm^2 for $\lambda = 526$ nm (cf. Fig. 2). The experimental threshold fluences for the sub-picosecond laser pulses[1] are: 2–2.5 J/cm^2 ($\lambda = 1053$ nm), ~ 2 J/cm^2 ($\lambda = 825$ nm), and 1.2–1.5 J/cm^2 ($\lambda = 526$ nm).

Using the following parameters for the fused silica at wavelength of 825 nm ($\kappa = 0.0087$ cm^2/s, ε_b
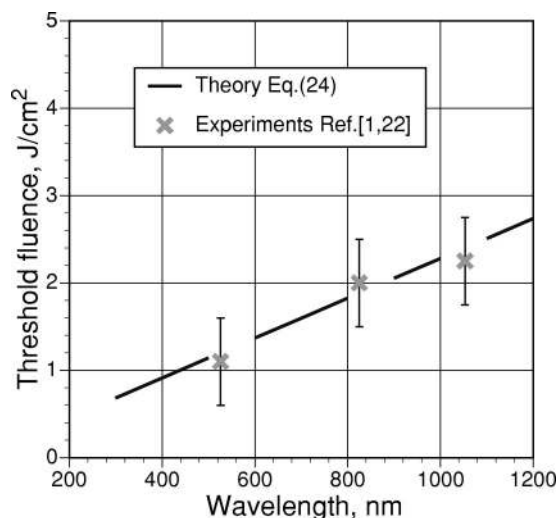
FIG. 2. Threshold fluence for laser ablation of fused silica target as a function of the laser wavelength for sub-picosecond laser pulses. The experimental points are from Refs. 1, 22.

$=3.7$ eV/atom; $n_a=0.7\times10^{23}$ cm^{-3}; and $A\sim3\times10^{-3}$) one obtains a good agreement with the experimental data collected in Ref. 1 for the laser pulse duration from 10 ps to 1 ns. The long pulse regime Eq. (26) holds: F_{th}[J/cm^2] $=1.29\times(t_p$[ps]$)^{1/2}$ (see Fig. 3).

The ablation threshold of 4.9 J/cm^2 for a fused silica with the laser $t_p=5$ fs, $\lambda=780$ nm, intensity$\sim10^{15}$ W/cm^2 has been reported in Ref. 23. This value is almost three times higher than that of Refs. 1, 22 and from the prediction of Eq. (24). However, the absorption coefficient as well as the pre-pulse to main pulse contrast ratio was not specified in Ref. 23.

In the Ref. 24 the crater depth of 120 nm was drilled in a BK7 glass by a 100-fs 620-nm laser at the intensity 1.5 $\times10^{14}$ W/cm^2. Assuming that the number density, the binding and the ionization energy in the BK7 glass target are the same as in fused silica, Eq. (27) for the ablation depth predicts the threshold value of 1.0 J/cm^2. This is in a reasonable
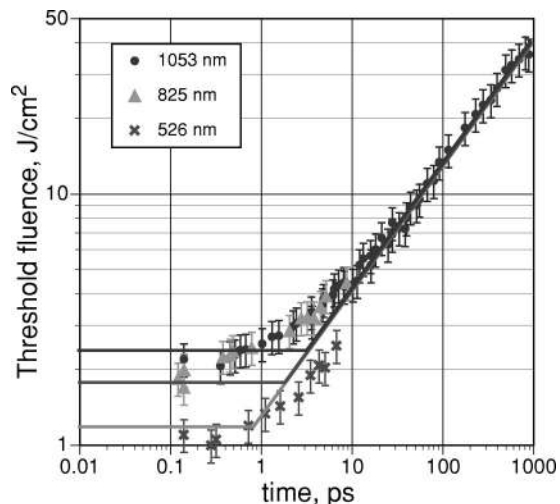
agreement with the measured in Ref. 24: $F_{th}=1.4$ J/cm^2. Equation (24) predicts $F_{th}=1.34$ J/cm^2 for this experiment.

It should be noted that the definition of the ablation threshold implies that at the threshold condition at least a mono-atomic layer $x\ll l_s$, of the target material should be removed. Therefore, the most reliable experimental data for the ablation threshold are those obtained by the extrapolation of the experimental dependence of the ablated depth versus the laser fluence to the "zero" depth. As one can see from above comparison, the experimental data on the ablation threshold determined this way are in excellent agreement with the formulas in this paper. It should be particularly emphasized that there were not any fitting coefficients in the calculations presented here.

XI. DISCUSSION AND CONCLUSIONS

We described here a new regime of material ablation in the ultra short laser-matter interaction mode. The regime is characterized by the laser intensity in the range of 10^{13} to 10^{14} W/cm^2 and the pulse duration shorter than the plasma expansion time, the heat conduction time, and the electron-to-ion energy transfer time. The interaction at such conditions results in ionization of practically any target material. The interaction with the metals and dielectrics proceeds in a similar way in contrast to the conventional, long pulse interaction mode. The physics of this new regime of ablation consists in the ion acceleration in the electrostatic field created by hot electrons escaping from the target. We derived the explicit analytical formulas for the ablation threshold, the electron temperature in the skin layer, and the ablation rates for metals and dielectrics in terms of laser and target parameters. These formulas do not contain any fitting parameters and agree well with the available experimental data. In this new regime the threshold fluence is almost independent on the pulse duration, and the material evaporation rate is much higher than in the long pulse interaction regime.

An important condition for the ultra short pulse interaction mode in the real experiments is the high contrast ratio of the pulse: the target surface should not be ionized, damaged or ablated during the pre-pulse action. For the nanosecond-scale pre-pulse and the 100 fs main pulse the intensity contrast ratio must be of the order of $\sim10^6$. The ultra short laser ablation can do a variety of fine jobs without any collateral damage to the rest of a target: cutting and drilling holes with a high precision, ablating all available materials with the ablation rate of several orders of magnitude faster than that with nanosecond lasers. The application of the ultra short lasers with high repetition rate for film deposition allows totally eliminate the problem of droplets and particulates on the deposited film. The theoretical background developed in this paper for laser ablation allows the appropriate laser parameters to be chosen for any given material and the laser-target interaction process to be optimized.

FIG. 3. Threshold laser fluence for ablation of fused silica target versus laser pulse duration. The experimental points are from Refs. 1, 22.

[1] M. D. Perry, B. C. Stuart, P. S. Banks, M. D. Feit, V. Yanovsky, and A. M. Rubenchik, J. Appl. Phys. **85**, 6803 (1999).
[2] D. Du, X. Liu, G. Korn, J. Squier, and G. Mourou, Appl. Phys. Lett. **64**, 3071 (1994); B. C. Stuart, M. D. Feit, A. M. Rubenchik, B. W. Shore, and M. D. Perry, Phys. Rev. Lett. **74**, 2248 (1995).

[3] E. G. Gamaly, A. V. Rode, and B. Luther-Davies, J. Appl. Phys. **85**, 4213 (1999); A. V. Rode, B. Luther-Davies, and E. G. Gamaly, *ibid.* **85**, 4222 (1999).

[4] P. Maine, D. Strickland, P. Bado, M. Pessot, and G. Mourou, IEEE J. Quantum Electron. **24**, 398 (1988).

[5] J. Squier, F. Salin, G. Mourou, and D. Harter, Opt. Lett. **16**, 324 (1991).

[6] E. G. Gamaly and V. T. Tikhonchuk, JETP Lett. **48**, 453 (1988).

[7] W. Rozmus and V. T. Tikhonchuk, Phys. Rev. A **42**, 7401 (1990); **46**, 7810 (1992).

[8] B. Luther-Davies, E. G. Gamaly, Y. Wang, A. V. Rode, and V. T. Tikhonchuk, Sov. J. Quantum Electron. **22**, 289 (1992).

[9] E. M. Lifshitz and L. P. Pitaevskii, *Physical Kinetics* (Pergamon, Oxford, 1981).

[10] L. D. Landau and E. M. Lifshitz, *Electrodynamics of Continuous Media* (Pergamon, Oxford, 1960).

[11] Yu. P. Raizer, *Laser-Induced Discharge Phenomena* (Consultant Bureau, New York, 1977).

[12] Yu. A Il'insky and L. V. Keldysh, *Electromagnetic Response of Material Media* (Plenum, New York, 1994).

[13] W. L. Kruer, *The Physics of Laser Plasma Interaction* (Addison Wesley, New York, 1987).

[14] Y. T. Lee and R. M. More, Phys. Fluids **27**, 1273 (1984).

[15] K. Eidmann, J. Meyer-ter-Vehn, T. Schlegel, and S. Huller, Phys. Rev. E **62**, 1202 (2000).

[16] C. Kittel, *Introduction to Solid State Physics*, 5th ed. (Wiley, New York, 1976).

[17] A. M. Malvezzi, N. Bloembergen, and C. Y. Huang, Phys. Rev. Lett. **57**, 146 (1986).

[18] E. G. Gamaly, Phys. Fluids B **5**, 944 (1993).

[19] V. Yu. Bychenkov, V. T. Tikhonchuk, and S. V. Tolokonnikov, Sov. Phys. JETP **88**, 1137 (1999).

[20] Yu. V. Afanasiev and O. N. Krokhin, "High temperature plasma phenomena during the powerful laser-matter interaction, in *Physics of High Energy Density*, Proceedings of the International School of Physics "Enrico Fermi" Course XLVIII, edited by P. Calderola and H. Knoepfel (Academic, New York, 1971); S. I. Anisimov, Y. A. Imas, G. S. Romanov, and Yu. V. Khodyko, *Action of High Power Radiation on Metals* (National Tech. Inform. Service, Springfield, VA, 1971).

[21] C. Momma, S. Nolte, B. N. Chichkov, F. V. Alvensleben, and A. Tunnermann, Appl. Surf. Sci. **109/110**, 15 (1997).

[22] B. C. Stuart, M. D. Feit, S. Herman, A. M. Rubenchik, B. W. Shore, and M. D. Perry, J. Opt. Soc. Am. B **13**, 459 (1996).

[23] M. Lenzner, J. Kruger, W. Kautek, and F. Krausz, Appl. Phys. A: Mater. Sci. Process. **69**, 465 (1999).

[24] K. Sokolowski-Tinten, J. Bialkowski, A. Cavalieri, M. Boing, H. Schuler, and D. von der Linde, Proc. SPIE **3343**, 47 (1998).

[25] R. B. Sosman, *The Phases of Silica* (Rutgers University Press, New Brunswick, NJ, 1965).